ISSN 0915-633X

NATIONAL INSTITUTE FOR FUSION SCIENCE

Macroscale Particle Simulation of Externally Driven Magnetic Reconnection

S. Murakami and T. Sato

(Received – Aug. 26, 1991)

NIFS-107 Sep. 1991

RESEARCH REPORT
NIFS Series

NAGOYA, JAPAN

Macroscale Particle Simulation of Externally Driven Magnetic Reconnection

Sadayoshi MURAKAMI* and Tetsuya SATO

Theory and Computer Simulation Center, National Institute for Fusion Science, Furou-cho, Chikusaku, Nagoya 464-01

Externally driven reconnection, assuming an anomalous particle collision model, is numerically studied by means of a 2.5D *macroscale particle simulation code* in which the field and particle motions are solved self-consistently. Explosive magnetic reconnection and energy conversion are observed as a result of slow shock formation. Electron and ion distribution functions exhibit large bulk acceleration and heating of the plasma. Simulation runs with different collision parameters suggest that the development of reconnection, particle acceleration and heating do not significantly depend on the parameters of the collision model.

Keywords : externally driven reconnection, macroscale particle simulation, slow shock, plasma acceleration and heating

*On leave from Faculty of Science, Hiroshima University.

§1. Introduction

Magnetic reconnection is a process by which the magnetic field line topology is changed and the magnetically stored energy is released to the plasma kinetic energy. The topology change of the magnetic field lines, which means the local breakdown of the frozen-in condition, leads to a global change of the plasma configuration and an enhanced transport along the reconnected field lines. In addition to this, the energy conversion causes a global change of the energy state. Thus, it seems that magnetic reconnection plays a key role in many energy relaxation processes in space and laboratory plasmas. Particularly, externally driven magnetic reconnection can convert the magnetic energy into the plasma energy in a much shorter time than the resistive diffusion. It is considered a most plausible mechanism of explosive energy release phenomena such as the solar flares, magnetospheric substorms and tokamak disruptions.

A theoretical model of magnetic reconnection, purely annihilation model, was suggested first by Sweet[1] and Parker[2], but the reconnection rate depends strongly on the electrical resistivity and is too small to explain the rapid solar flares. In the meantime, Petschek[3] pointed out the importance of the role of the magnetohydrodynamic(MHD) wave in the downstream and suggested a fast reconnection rate to account for the rapid energy conversion rate. His model was modified by Sonnerup[4] and Yeh and Axford[5] based on a dimensional analysis.

Numerical simulation has played a leading role in understanding the dynamical behaviors of the magnetic reconnection process. The importance of an externally *driven* reconnection was first pointed by Sato and Hayashi using a 2D MHD simulation[6–9]. They show that the externally driven reconnection process converts the free magnetic energy to the plasma kinetic energy(acceleration and heating) in a time scale much faster than the resistive diffusion time

as a result of slow shock formation. It is also pointed out that resistivity (internal condition) acts as a catalysis in the development of reconnection and the driving plasma flow(external condition) governs the whole evolution.

Through research efforts by many[10–12], the global behavior of the magnetic reconnection process has become more understood. However, kinetic behaviors of electrons and ions remain unclarified, e.g., generation of energetic particles in the magnetotail and anomalous ion heating in the reversed field pinch (RFP)[13]. Single particle motions are studied in the static field[14] and in the space- and time-varying field[15]. In the plasma, however, the particle motions and fields are inseparable and self-interacting. Therefore, in order to have a complete understanding of particle acceleration and heating in the reconnection process a self-consistent study of the fields and particles is required.

In this paper, we numerically study the externally driven reconnection by means of a two and a half dimensional (2.5D) *macroscale particle simulation code* in which the field and particle motions are solved self-consistently. The *macroscale particle simulation code*[16–19] is so programmed that kinetic processes interacting with magnetohydrodynamic processes can be treated.

In order to simulate a fully self-consistent driven reconnection where collisionless dissipation or anomalous resistivity can be spontaneously taken into account, three dimensional behaviors must be considered. In the present 2.5D model where the variations along the neutral sheet current are ignored, collisionless dissipation can not adequately be dealt with. We thus introduce an anomalous collision model such that the collision frequency is dependent upon the magnitude of the neutral sheet current. Specifically, we assume that some microscopic current driven instability occurs when the neutral sheet current is locally enhanced by compression due to a converging driving flow and exceeds a certain threshold.

In section 2 the fundamental equations, the initial condition, the boundary condition and the particle collision model are described. In section 3 the results of five representative simulation runs are shown. First, we see the development of driven reconnection, and acceleration and heating of the plasma for a typical case and, then, investigate the influence of the particle collision frequency and threshold current on the reconnection process, along with the particle acceleration and heating by examining the temporal change of the particle distribution functions. Conclusion is given in section 4.

§2. Simulation Model

In order to cover the MHD space and time behaviors along with the particle kinetics, we use a 2.5D *macroscale particle simulation code*, in which the time-decentered discretization technique is used both in the equations of particles and fields, in other words, implicit source terms are introduced in the field-particle coupled equations. By using this technique and taking a large time step one can damp out arbitrarily high frequency modes and thus desired low frequency phenomena can practically be dealt with.

The equations to be solved are a full set of Maxwell's equations, namely,

$$\nabla \times \mathbf{E} = -\frac{1}{c}\frac{\partial \mathbf{B}}{\partial t}, \tag{1}$$

$$\nabla \times \mathbf{B} = \frac{1}{c}\frac{\partial \mathbf{E}}{\partial t} + \frac{4\pi}{c}\mathbf{j}, \tag{2}$$

$$\nabla \cdot \mathbf{E} = 4\pi\rho, \tag{3}$$

$$\nabla \cdot \mathbf{B} = 0, \tag{4}$$

and the equations of motion for electrons and ions, namely,

$$m_s\frac{d\mathbf{v}}{dt} = q_s[\mathbf{E}(\mathbf{x}) + \frac{1}{c}\mathbf{v} \times \mathbf{B}(\mathbf{x})], \tag{5}$$

$$\frac{d\mathbf{x}}{dt} = \mathbf{v}, \tag{6}$$

where $\mathbf{x}, \mathbf{v}, q_s$ and m_s are the position vector, the velocity, the charge and the mass of a particle, respectively, and the subscript s denotes the particle species (electron or ion). The current density $\mathbf{j}$ and the charge density ρ are defined by summing up all the particles,

$$\mathbf{j}(\mathbf{x},t) = \sum_s \sum_j q_s \mathbf{v}_j(t) S[\mathbf{x} - \mathbf{x}_j(t)], \tag{7}$$

$$\rho(\mathbf{x},t) = \sum_s \sum_j q_s S[\mathbf{x} - \mathbf{x}_j(t)], \tag{8}$$

where $S[\mathbf{x}]$ is a shape function to assign the particle quantity to the neighboring field grids. We numerically solve the time evolution of these field-particle coupled equations, eqs. (1),(2),(5), (6) and (7). Equations (3) and (4) are initially satisfied. Homogeneity in z-direction($\partial/\partial z = 0$) and symmetry (anti-symmetry) about the x and y axis are assumed. In actual simulations we solve these equations only on one quarter of the x-y plane by the symmetrical or anti-symmetrical condition.

The initial plasma condition is set to satisfy the following MHD equilibrium condition:

$$\mathbf{j} \times \mathbf{B} = \nabla p, \tag{9}$$

where an isotropic pressure profile p is assumed. Actually, we use a Harris-type antiparallel magnetic field configuration in which the magnetic field has only the x component and the amplitude varies only along the y axis as

$$B_x(y) = B_0 \tanh(y/L). \tag{10}$$

The current $j(y)$ and the pressure $p(y)$ are

$$j_z(y) = j_0 \mathrm{sech}^2(y/L), \tag{11}$$

$$p(y) = p_0 \mathrm{sech}^2(y/L), \tag{12}$$

where $j_0 = cB_0/4\pi L$, $p_0 = cB_0^2/8\pi$, and L is the characteristic length of the initial configuration. We have assumed the electric field to be zero initially in the entire simulation box. The densities of electrons and ions, ρ_e and ρ_i, are assumed uniform and satisfy the neutral condition($\rho = q_e\rho_e + q_i\rho_i = 0$). The electron temperature T_e is assumed to be equal to the ion temperature T_i. Consequently, the pressure of the electron and ion are the same and the pressure gradient is equivalent to the temperature gradient.

In the actual calculations all variables are normalized by using the following four basic units: ω_{pe} (electron plasma frequency), c (speed of light), m_e (electron mass), and e (electron charge). Accordingly, the time, the length, the electric field, and the magnetic field are normalized by ω_{pe}^{-1}, c/ω_{pe}, $m_e c\omega_{pe}/e$, $m_e c\omega_{pe}/e$, respectively.

The actual simulation system is a rectangular box surrounded by four planes, $x = 0$, $x = L_x$, $y = 0$ and $y = L_y$. This is implemented on a 61×61 point grid. The boundary plane at $y = L_y$ is the input boundary through which a plasma flows in. More specifically, we apply an electric field in the negative z direction at $y = L_y$ and drive the plasma toward the neutral sheet by the $E \times B$ drift. The electric field applied at the input boundary, $E_{i.b.}$, is given by

$$E_{i.b.}(x) = \begin{cases} -\frac{E_0}{2}(1 + \cos\frac{x-\delta}{L_x-\delta}\pi) & for \quad \delta \le x \le L_x, \\ -E_0 & for \quad 0 \le x \le \delta. \end{cases} \tag{13}$$

The electric field, E_0, is increased monotonically in time and fixed to E_0 at $T = 4000\omega_{pe}^{-1}$, which is roughly $2\tau_A$ where τ_A is the Alfven transit time.

The boundary located at $x = L_x$ is the output boundary. The condition of the output boundary consists of the following two conditions. One is the particle condition such that the particles can freely get in and out and the other is the field condition that the waves can be absorbed there (no reflection). In order to satisfy these conditions we set an extra damping

region beyond the output boundary.

Let us now describe our collision model. The initial plasma is assumed a collisionless plasma, so that no resistivity exists in the plasma. But, since the neutral sheet plasma is compressed by the plasma inflow given by eq. (13), the neutral sheet current around the origin is strengthened with time. It is supposed, therefore, that some microscopic current driven instability will be eventually generated, whereby electrons and ions will be scattered by unstable waves. For the sake of simplicity and conservation of the particle energy by each collision, we adopt such a collision model that scattering of electrons and ions by unstable waves takes place only in the z-direction (in the direction of the neutral sheet current). The model collision frequencies for electrons and ions we take in this study are given by

$$\nu_s = \begin{cases} \nu_0 \alpha_s (j - j_c)^2 / j_0^2 & for \quad j \geq j_c, \\ 0 & for \quad j < j_c, \end{cases} \tag{14}$$

where j_c is the threshold current and α_s is a properly chosen constant. The subscript s denotes the particle species. This collision model conserves the total momentum by collisions.

§3. Simulation Results

Simulation parameters are as follows: the mass ratio is $m_i/m_e = 40$, the magnetic field intensity is $B_0 = 0.3 m_e c\omega_{pe}/e$, the characteristic length is $L = 100c/\omega_{pe}$, the simulation box dimension is $L_x = 300c/\omega_{pe}$ and $L_y = 200c/\omega_{pe}$. The Alfven transit time $\tau_A (= L/V_A)$ becomes $2134\omega_{pe}^{-1}$ for these parameters. The electric field at the input boundary E_{ib} is $4.0 \times 10^{-3} m_e c\omega_{pe}/e$ and the maximum input flow speed is $0.28 V_A$.

Five parameter runs (A-E) with different particle collision frequencies ν_0 and threshold currents j_c, which are given in Table I, are performed with intent to investigate the influence on the development of reconnection and the plasma acceleration and heating. Case D

corresponds to a high threshold current and case E to a collisionless case in which no model collision is introduced.

In what follows we first show how the reconnection process and the acceleration and heating of plasma progress for a typical case(case A). Then we show the influence of the particle collision frequency and the threshold current on the development of the reconnection process and the particle acceleration and heating.

§3.1 *Development of reconnection*

The temporal evolutions of the magnetic field line topology (contour plots of the vector potential) and the plasma flow velocity for the four quadrants are shown in Fig. 1. The left panels present the temporal evolution of the magnetic field lines and the right panels present that of the plasma flow velocity. The flow velocity is normalized by half of the Alfven speed defined by the magnetic field and the density at the initial input boundary. The magnitude of this speed is indicated at the top-right corner of each panel.

We start the simulation run with the MHD Harris-type equilibrium. We apply an electric field at the input boundary so that the plasma can gradually squeeze into the simulation box by the $E \times B$ drift. At $T = 2000\omega_{pe}^{-1}$, the plasma flow is found to have reached to the neutral sheet. At $T = 10000\omega_{pe}^{-1}$ the magnetic field lines are observed to bend concavely toward the neutral sheet. Reconnection has not yet begun at this stage. At $T = 20000\omega_{pe}^{-1}$ the magnetic field lines start to reconnect and the reconnected field lines are removed toward the output boundary from the reconnection point by the plasma flow generated by the $\mathbf{j} \times \mathbf{B}$ force. The magnetic reconnection process reaches almost to a steady state at $T = 30000\omega_{pe}^{-1}$ where a large plasma flow is generated. Formation of the slow shock, which can be recognized by the abrupt bending of the field lines, is observed in the downstream region. The rapid plasma

acceleration occurs when the plasma passes through the slow shock and the maximum flow velocity of the plasma in the downstream region reaches up to 0.7 V_A.

Figure 2 shows the three dimensional plots of the current development for the four quadrants. At $T = 10000\omega_{pe}^{-1}$ a slight current intensification appears near the most flow converging point (origin) in the neutral sheet, though its value is yet less than the threshold current. The current eventually exceeds the threshold current and rapid reconnection starts at about $T = 19000\omega_{pe}^{-1}$. As the reconnection develops, the current sheet changes its structure. At $T = 29200\omega_{pe}^{-1}$ an X type current sheet structure develops roughly along the magnetic separatrix. This X type current sheet structure indicates the formation of slow shock.

Three dimensional plots of the development of the pressure profile are shown in Fig. 3. The pressure is peaked at the center of the neutral sheet at $T = 10000\omega_{pe}^{-1}$. The induced pressure gradient causes the plasma to flow out toward the output boundaries. At $T = 18200\omega_{pe}^{-1}$ reconnection gets started and the pressure gradually increases at the reconnection point and also in the downstream region. At $T = 29800\omega_{pe}^{-1}$ the pressure increases further in the downstream but slightly decreases near the reconnection point.

Figure 4 shows the temporal development of the contours of the electric field E_z. The distribution of the electric field intensity along the x axis at $y = 0$ is shown in the upper margin and the distribution along the y axis at $x = 0$ is shown in the right margin. At $T = 2000\omega_{pe}^{-1}$, the electric field, which was none initially, penetrates deep into the neutral sheet. At $T = 10000\omega_{pe}^{-1}$ the plasma flow reaches almost to a maximum value. However, the current has not yet reached to the threshold current, thus, the electric field at the reconnection point yet remains null. At about $T = 20000\omega_{pe}^{-1}$ the current exceeds the threshold current, and hence, the resistivity caused by particle collisions starts to generate the electric field at the reconnection point. When time further elapses and reaches $T = 30000\omega_{pe}^{-1}$, the electric

field E_z becomes almost uniform in the entire region, this indicating that the magnetic reconnection process attains a steady state.

§3.2 *Acceleration and heating of electrons and ions*

In this subsection we shall concentrate on the acceleration and heating of electrons and ions.

The flow velocities and temperatures of electrons and ions at $T = 30000\omega_{pe}^{-1}$ are shown in Fig. 5; (a) for electrons and (b) for ions. The flow velocity is normalized by half of the Alfven speed defined by the initial input boundary values. It is found that the patterns of the electron and ion flow velocities are nearly the same and rapid accelerations takes place when the particles encounter the slow shock. The temperature profiles indicate large heating of both electrons and ions in the downstream of the slow shock. It is interesting to observe that the spatial structure of the electron temperature has a steeper profile than that of the ion temperature and that the temperature peak appears near $x = 100c/\omega_{pe}$ rather than the X point.

We shall now examine the details of the electron and ion distribution functions. Figure 6 shows the electron and ion velocity distribution functions at $T = 30971\omega_{pe}^{-1}$ on the upstream and downstream sides of the slow shock; (a) for electrons and (b) for ions. The dashed line indicates the average velocity on the downstream side. The particle distribution is very sharp in the upstream, while in the downstream the distribution becomes much broader. This broadening of the distribution function indicates strong heating of electrons and ions by reconnection. Particularly, the ion distribution has a long tail in the high velocity region than that of electrons. Acceleration of plasmas can be identified by the shift of the distribution function. A large shift for the ion v_x distribution function and a small shift for the

electron v_x distribution are found, which indicates that ions are more efficiently accelerated by reconnection.

From the above examination of the particle behaviors it is concluded that large acceleration and heating are caused by externally driven magnetic reconnection.

§3.3 *Influence of particle collisions on the reconnection process*

Since we have known an overall view of the development of reconnection and associated plasma acceleration and heating for one case, we shall next examine the influence of the collision model on the development of the reconnection process.

In doing so, we shall first see the results of collisionless case (case E) where no model collision is introduced. By the plasma compression due to the presence of a converging driving force the pressure and current become steepened near the central region, but no significant reconnection is observed. This result implies that the numerical collision is ignorable in our simulations.

Figure 7 shows the development of the reconnection rate for three different particle collision frequencies, namely, (A) $\nu_0 = 2.7 \times 10^{-3}$, (B) $\nu_0 = 1.8 \times 10^{-3}$ and (C) $\nu_0 = 0.9 \times 10^{-3}$, but remaining the other parameters the same. We evaluate the reconnection rate by the value of $\mathbf{V} \times \mathbf{B}$ (the magnetic flux passing in the unit time, or the reconnection electric field) at the fixed point in the downstream region ($y = 0, x = 64c/\omega_{pe}$). No significant differences are observed about the development of the reconnection rate. This leads us to a conclusion that the development of reconnection is rather independent of the strength of the collision ν_0.

Figure 8 shows the electron and ion distribution functions in the downstream region for three different particle collision frequencies; (A) $\nu_0 = 2.7 \times 10^{-3}$, (B) $\nu_0 = 1.8 \times 10^{-3}$ and (C)

$\nu_0 = 0.9 \times 10^{-3}$. The left panels are the electron distribution functions in the downstream and the right panels are the ion distribution functions. The dashed line represents the average velocity. Rapid acceleration and heating of electrons and ions are observed but no remarkable differences are observed on the electron and ion distribution functions for all three cases. This result again confirms the above conclusion that plasma acceleration and heating are nearly independent of the collision frequency ν_0.

Figure 9 shows the development of the reconnection rate for two different threshold currents, namely, (A) $j_c = 4.0 \times 10^{-4}$ and (D) $j_c = 8.0 \times 10^{-4}$, with the other parameters remaining the same. No remarkable differences are again observed for two cases except for a slight time delay on the onset time of reconnection. This time delay of the onset time can well be explained by the fact that when the threshold current j_c is larger, it takes more time for the current to exceed the threshold current and for the anomalous resistivity to become substantial. This indicates that the development of reconnection is not intrinsically dependent on the value of the threshold current j_c.

Figure 10 shows the electron and ion distribution functions in the downstream for two different threshold currents; (A) $j_c = 4.0 \times 10^{-4}$ and (D) $j_c = 8.0 \times 10^{-4}$. The left panels show the electron distribution functions in the downstream and the right panels show the ion distribution functions. The dashed line is the average velocity. This result also supports the above conclusion that the acceleration and heating of plasmas are essentially independent of the value of the threshold current j_c.

We have studied the influences of collision parameters on the development behaviors of reconnection, acceleration and heating. Consequently, it is founded that the reconnection process, particularly, the plasma acceleration and heating, do little depend on collisions. This conclusion strongly supports the conclusion of the previous MHD simulation[9], namely

that the development of the driven reconnection process is a rather independent process of the resistivity and that the resistivity merely acts as a catalysis of a flow driven reconnection.

§4. Conclusion

By solving the field and particle motions self-consistently using a 2.5D *macroscale particle simulation code* we have been able to study a flow driven reconnection process, assuming an anomalous particle collision model.

A converging plasma flow toward a neutral sheet compresses the neutral sheet at a converging point. When the neutral current is strongly intensified there, some particle effect is expected to give rise to some collisionless dissipation. Reconnection would then be triggered there. In the present study using a 2.5D particle code, an anomalous collision model is adopted to model an anomalous collision effect due to local current intensification. It is found that when a neutral sheet is locally thinned by a conversing flow, collisions trigger reconnection and that reconnection gives rise to slow shocks whereby rapid acceleration and heating of electrons and ions take place. It is important to note that the rapid rise of the reconnection rate and associated heating and acceleration are almost independent of the collision model and much faster than the resistive time. This study not only confirms the validity of the previous MHD simulation results, but gives that electrons and ions are anomalously heated through the driven reconnection process.

Acknowledgements

The authors wish to thank Professors M. Tanaka, R. Horiuchi, K. Watanabe and T. Hayashi for their warm advice and guidance. Thanks are also due to Professor K. Nishikawa for his continuous encouragements and to Dr. Z. Yoshida for his valuable advice.

References

1) P. A. Sweet: Nuovo Cimento Suppl. **8**, Ser. **X** (1958) 188.

2) E. N. Parker: Astrophys. J. Suppl. Ser. **77** (1963) 177.

3) H. E. Petschek: AAS-NASA Symp., NASA SP-50 (1965) p. 425.

4) B. U. Ö. Sonnerup: J. Plasma Phys. **4** (1970) 161.

5) T. Yeh and W. I. Axford: J. Plasma Phys. **4** (1970) 207.

6) T. Hayashi and T. Sato: J. Geophys. Res. **83** (1978) 217.

7) T. Sato, T. Hayashi, T. Tamano and A. Hasegawa: Phys. Rev. Lett. **41** (1978) 1548.

8) T. Sato: J. Geophys. Res. **84** (1979) 7177.

9) T. Sato and T. Hayashi: Phys. Fluid **22** (1979) 1189.

10) V. M. Vasyliunas: Rev. Geophys. Space Phys. **13** (1975) 303.

11) B. K. Shivamoggi: Rhys. Rep. **127** (1985) 99.

12) B. U. Ö. Sonnerup: Computer Phys. Commun. **49** (1988) 143.

13) Z. Yoshida: Nucl. Fusion **31** (1991) 386.

14) T. W. Speiser and L. R. Lyons: J. Geophys. Res. **89** (1984) 147.

15) T. Sato, H. Matsumoto and K. Nagai: J. Geophys. Res. **87** (1982) 6089.

16) M. Tanaka and T. Sato: Phys. Fluids **29** (1986) 3823.

17) M. Tanaka, T. Sato and A. Hasegawa: Geophys. Rev. Lett. **14** (1987) 868.

18) M. Tanaka, T. Sato and A. Hasegawa: Phys. Fluids B1 (1989) 325.

19) R. Horiuchi and T. Sato: Phys. Fluids B2 (1990) 2652.

Figure Captions

Fig. 1 Temporal evolution of the magnetic field lines (contour plots of vector potential) and the plasma flow velocity.

Fig. 2 Three dimensional plots of the evolution of the current distribution; (a) $T = 200\omega_{pe}^{-1}$, (b) $T = 10000\omega_{pe}^{-1}$, (c) $T = 19000\omega_{pe}^{-1}$ and (d) $T = 29200\omega_{pe}^{-1}$. At $T = 29200\omega_{pe}^{-1}$, the X type current sheet structure indicates the formation of slow shock.

Fig. 3 Three dimensional plots of the pressure profile development; (a) $T = 200\omega_{pe}^{-1}$, (b) $T = 10000\omega_{pe}^{-1}$, (c) $T = 18200\omega_{pe}^{-1}$ and (d) $T = 29800\omega_{pe}^{-1}$.

Fig. 4 Temporal development of the contour of the electric field E_z; (a) $T = 2000\omega_{pe}^{-1}$, (b) $T = 10000\omega_{pe}^{-1}$, (c) $T = 20000\omega_{pe}^{-1}$ and (d) $T = 30000\omega_{pe}^{-1}$. The distributions along the x axis at $y = 0$ and along the y axis at $x = 0$ are shown in the upper and right margins, respectively.

Fig. 5 Plasma flow velocities and temperature profiles at $T = 30000\omega_{pe}^{-1}$; (a) for electrons and (b) for ions.

Fig. 6 Electron and ion distribution functions on the upstream and downstream sides of the slow shock at $T = 30971\omega_{pe}^{-1}$. The dashed line indicates the average velocity in the downstream.

Fig. 7 Development of the reconnection rate for three different particle collision frequencies; (A) $\nu_0 = 2.7 \times 10^{-3}$, (B) $\nu_0 = 1.8 \times 10^{-3}$ and (C) $\nu_0 = 0.9 \times 10^{-3}$. No remarkable difference is observed for the evolution of the reconnection rate.

Fig. 8 Electron and ion distribution functions in the downstream at $T = 30971\omega_{pe}^{-1}$ for three different particle collision frequencies; (A) $\nu_0 = 2.7 \times 10^{-3}$, (B) $\nu_0 = 1.8 \times 10^{-3}$ and (C) $\nu_0 = 0.9 \times 10^{-3}$.

Fig. 9 Time evolution of the reconnection rate for two different threshold currents; (A) $j_c = 4.0 \times 10^{-4}$ and (D) $j_c = 8.0 \times 10^{-4}$. No remarkable difference is observed on the evolution of the reconnection rate except for a slight time delay for the onset time of reconnection.

Fig. 10 Electron and ion distribution functions in the downstream for two different threshold currents; (A) $j_c = 4.0 \times 10^{-4}$ and (D) $j_c = 8.0 \times 10^{-4}$.

Table I: Collision parameters of five simulation runs.

Case	A	B	C	D	E
ν_0	2.7×10^{-3}	1.8×10^{-3}	0.9×10^{-3}	2.7×10^{-3}	0.0
j_c	4.0×10^{-4}	4.0×10^{-4}	4.0×10^{-4}	8.0×10^{-4}	—
Remarks				high j_c	collisionless

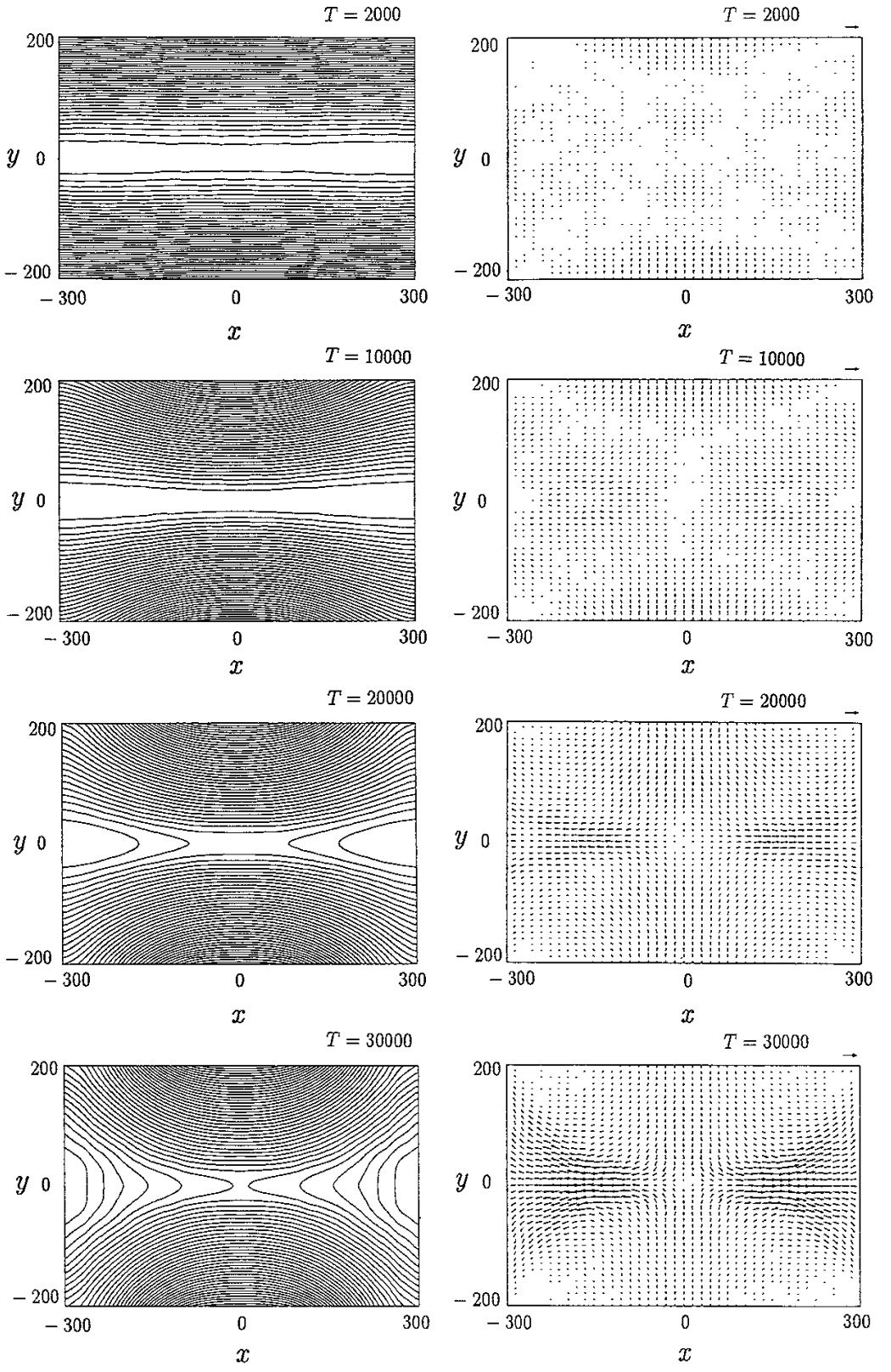
T = 2000
T = 2000
T = 10000
T = 10000
T = 20000
T = 20000
T = 30000
T = 30000
200
0
− 200
y
− 300
0
300
x

Fig. 1

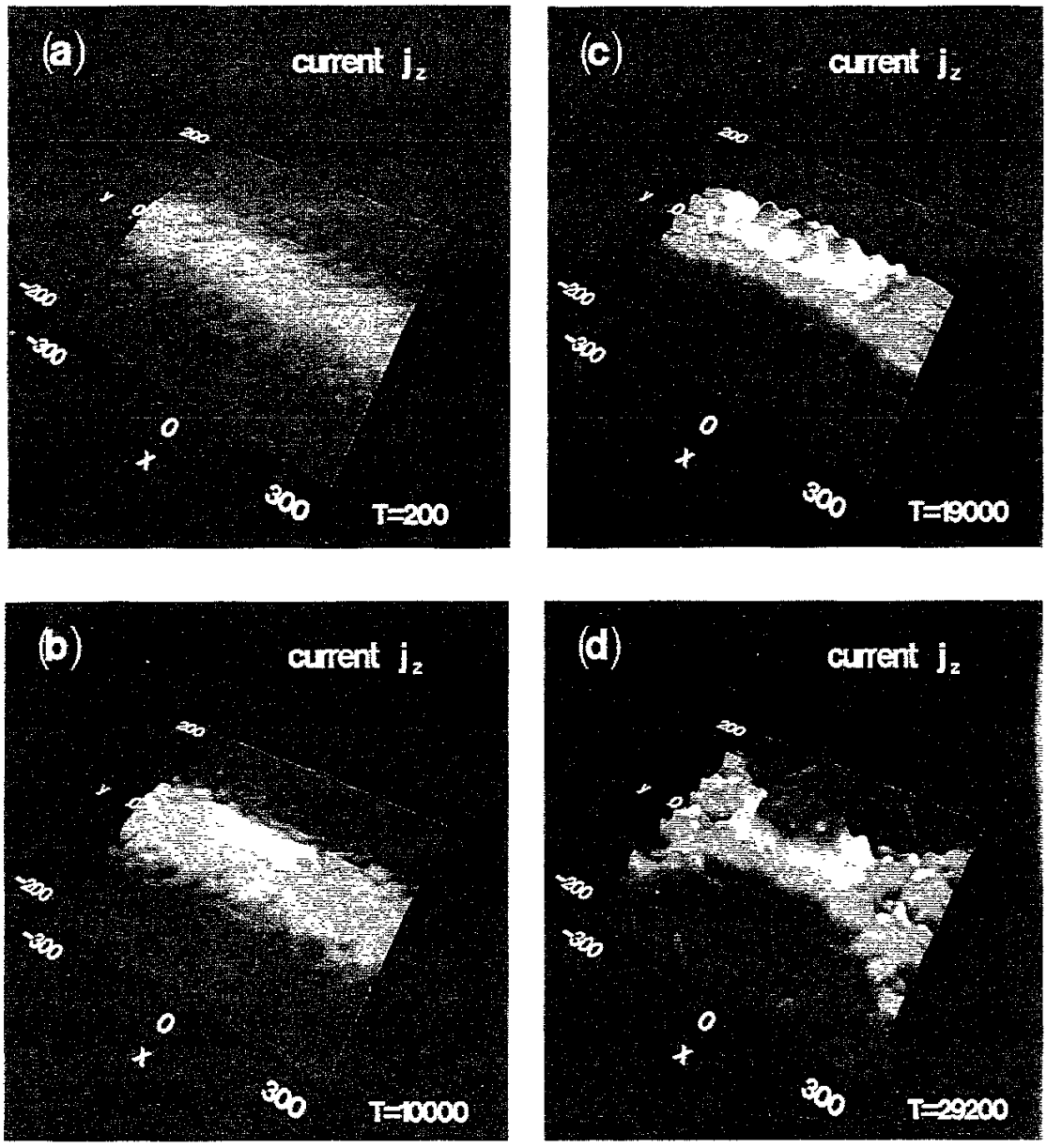
(a)
current j_z
200
y
0
-200
-300
0
x
300
T=200
(c)
current j_z
200
y
0
-200
-300
0
x
300
T=19000
(b)
current j_z
200
y
0
-200
-300
0
x
300
T=10000
(d)
current j_z
200
y
0
-200
-300
0
x
300
T=29200

Fig. 2

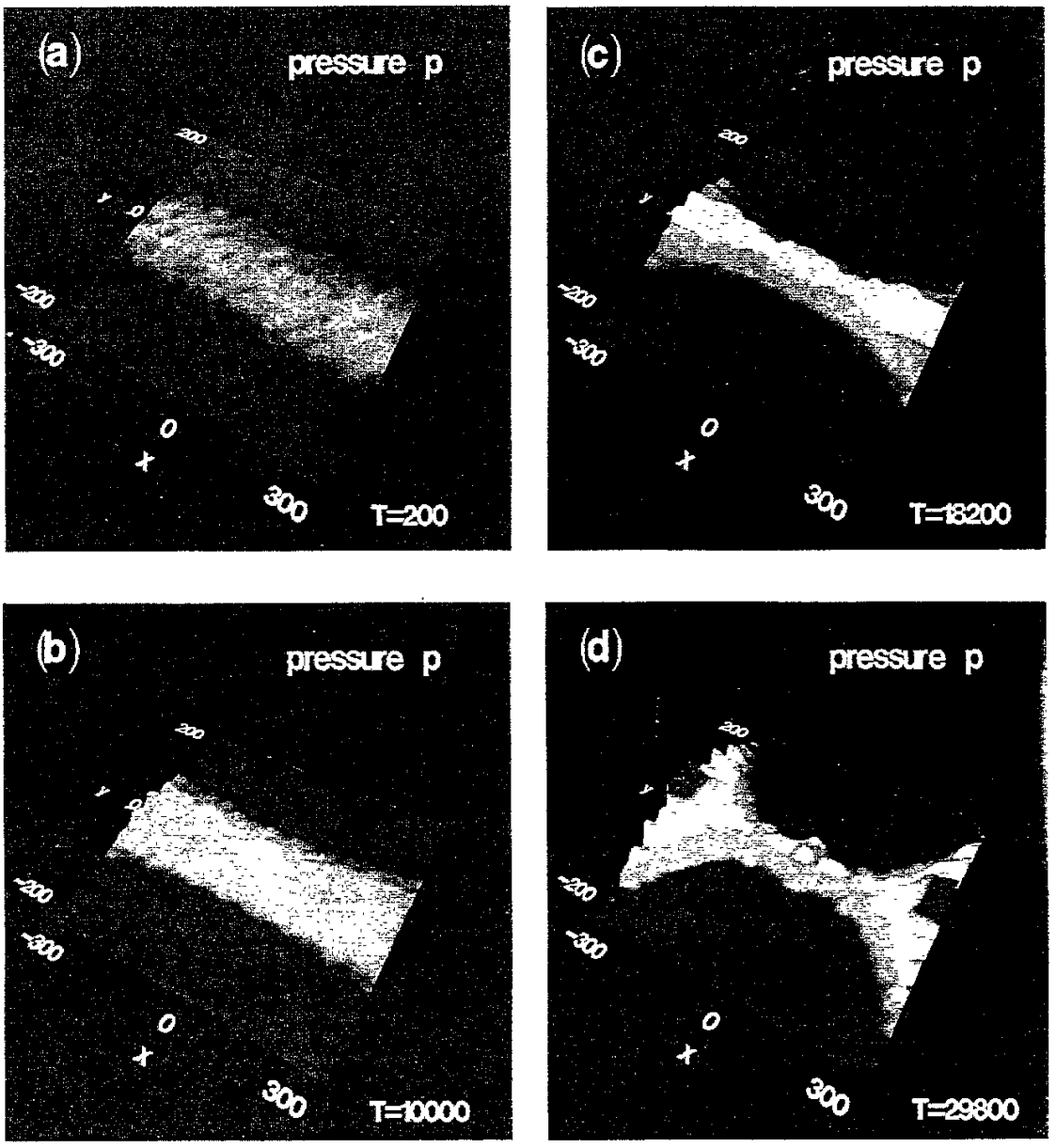
(a)
pressure p
200
y
0
-200
-300
0
x
300
T=200
(c)
pressure p
200
y
-200
-300
0
x
300
T=18200
(b)
pressure p
200
y
0
-200
-300
0
x
300
T=10000
(d)
pressure p
200
y
-200
-300
0
x
300
T=29800

Fig. 3

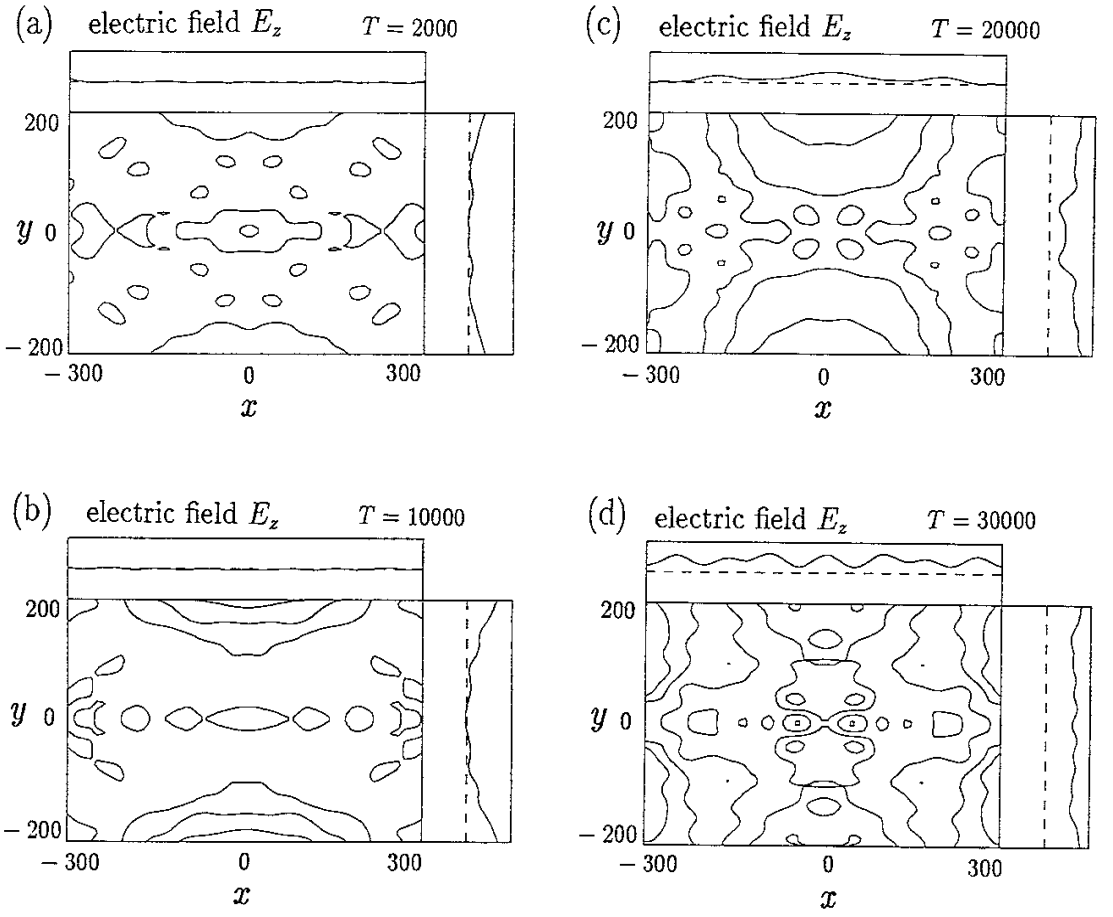
(a) electric field E_z $T = 2000$
(c) electric field E_z $T = 20000$
(b) electric field E_z $T = 10000$
(d) electric field E_z $T = 30000$
200
0
− 200
y
− 300
0
300
x

Fig. 4

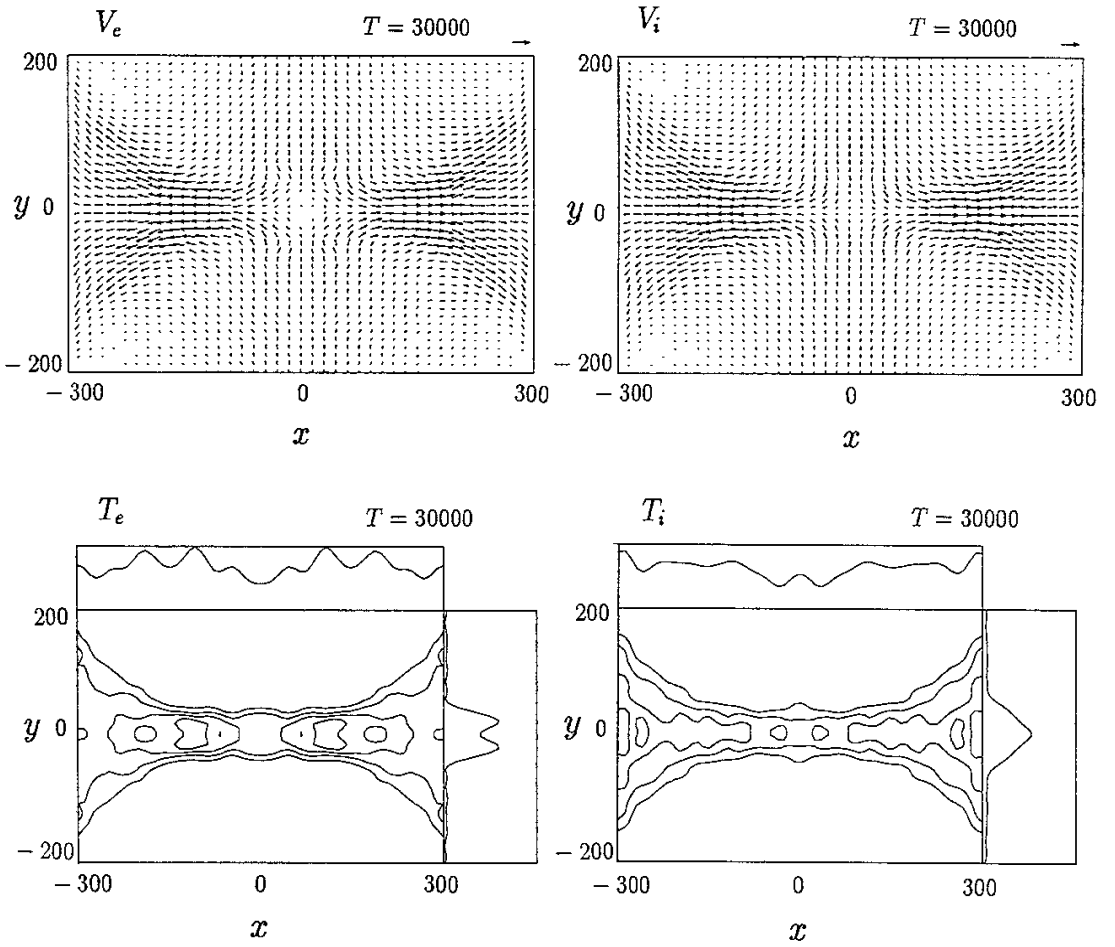
V_e
$T = 30000$
200
y 0
-200
-300
0
300
x
V_i
$T = 30000$
200
y 0
-200
-300
0
300
x
T_e
$T = 30000$
200
y 0
-200
-300
0
300
x
T_i
$T = 30000$
200
y 0
-200
-300
0
300
x

Fig. 5

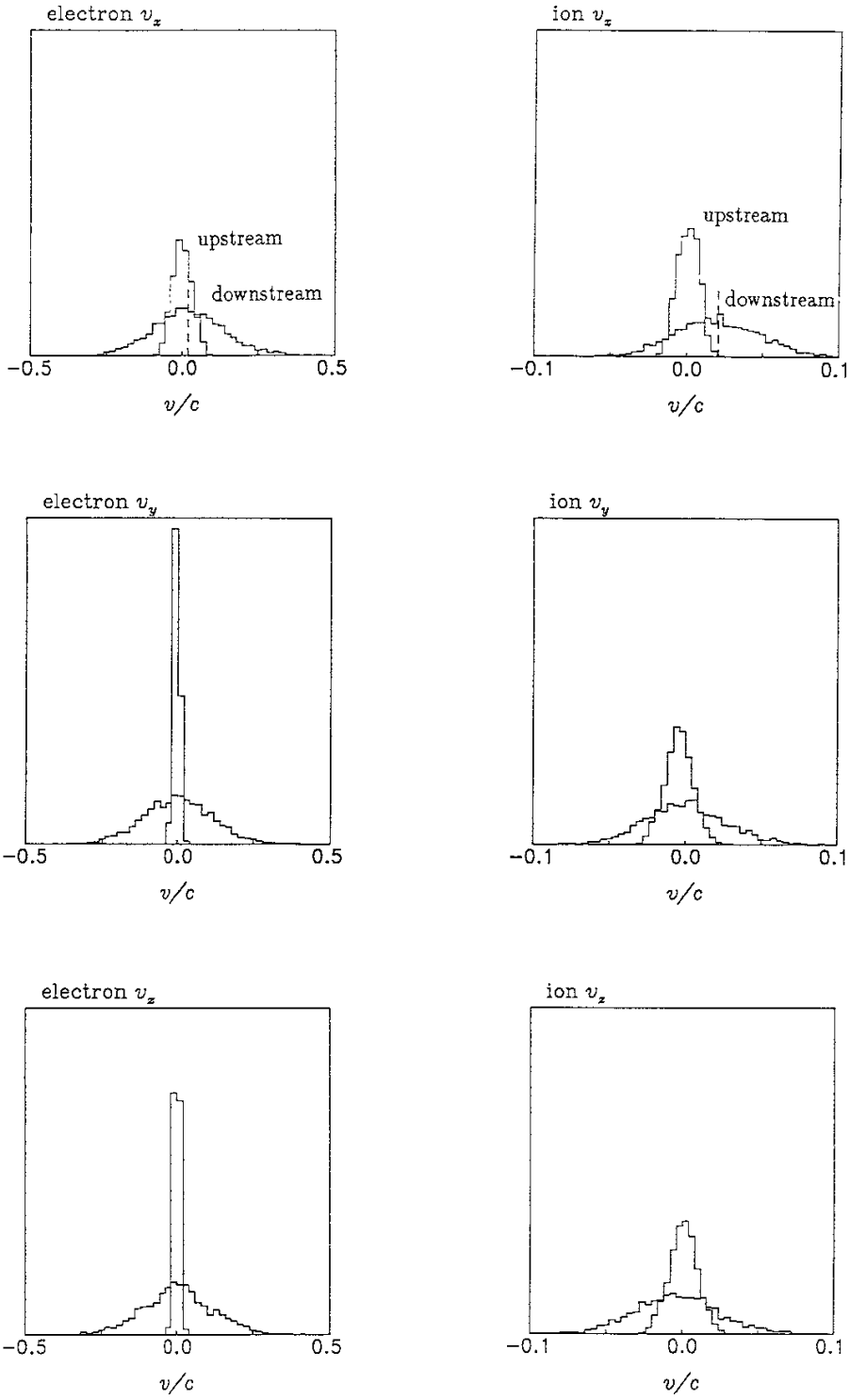
electron v_x
upstream
downstream
−0.5
0.0
0.5
v/c
ion v_x
upstream
downstream
−0.1
0.0
0.1
v/c
electron v_y
−0.5
0.0
0.5
v/c
ion v_y
−0.1
0.0
0.1
v/c
electron v_z
−0.5
0.0
0.5
v/c
ion v_z
−0.1
0.0
0.1
v/c

Fig. 6

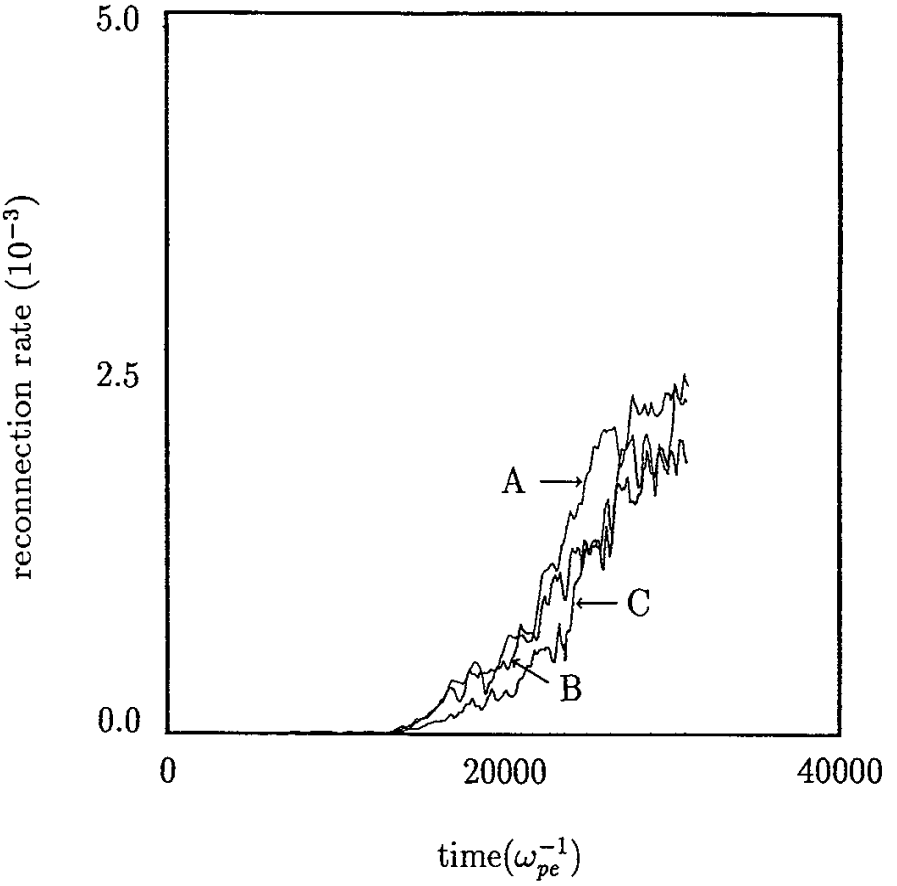
5.0
2.5
0.0
reconnection rate (10^{-3})
A
C
B
0
20000
40000
time(ω_{pe}^{-1})

Fig. 7

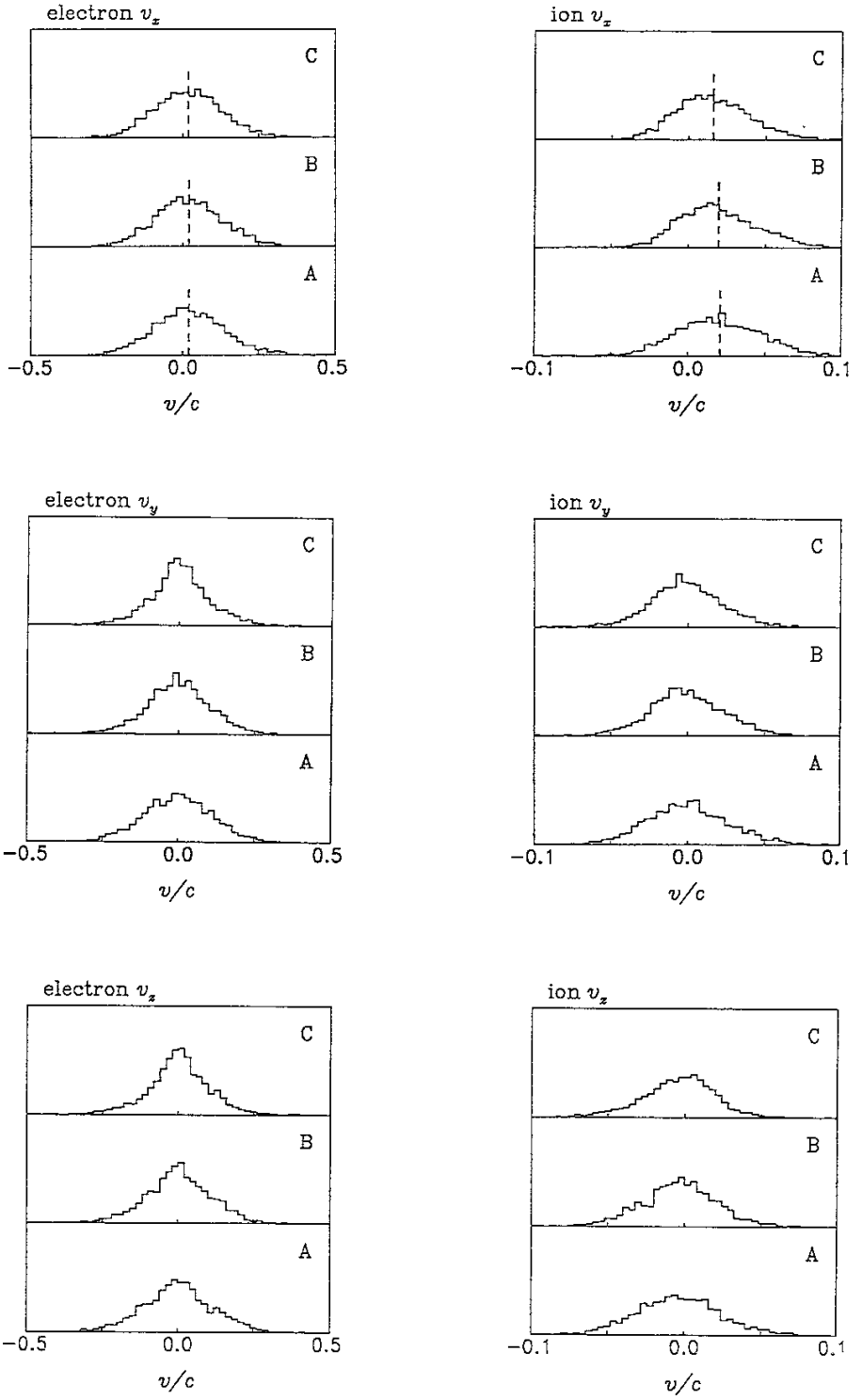
electron v_x
C
B
A
−0.5
0.0
0.5
v/c
ion v_x
C
B
A
−0.1
0.0
0.1
v/c
electron v_y
C
B
A
−0.5
0.0
0.5
v/c
ion v_y
C
B
A
−0.1
0.0
0.1
v/c
electron v_z
C
B
A
−0.5
0.0
0.5
v/c
ion v_z
C
B
A
−0.1
0.0
0.1
v/c

Fig. 8

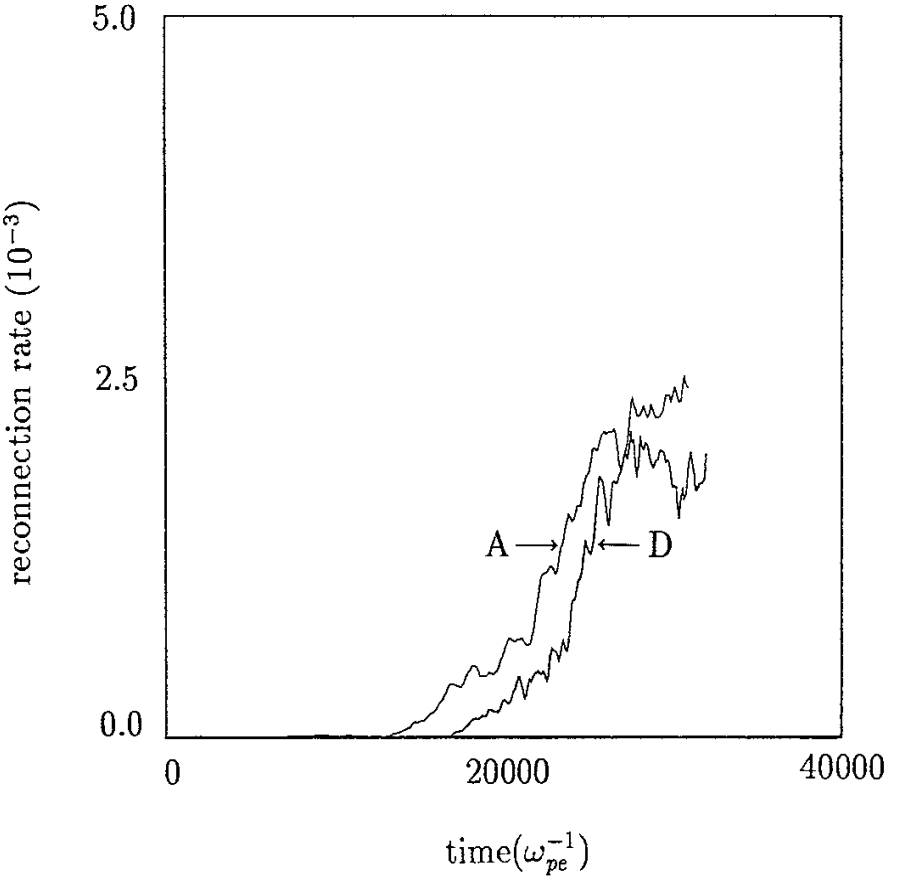
5.0
2.5
0.0
reconnection rate (10^{-3})
A
D
0
20000
40000
time(ω_{pe}^{-1})

Fig. 9

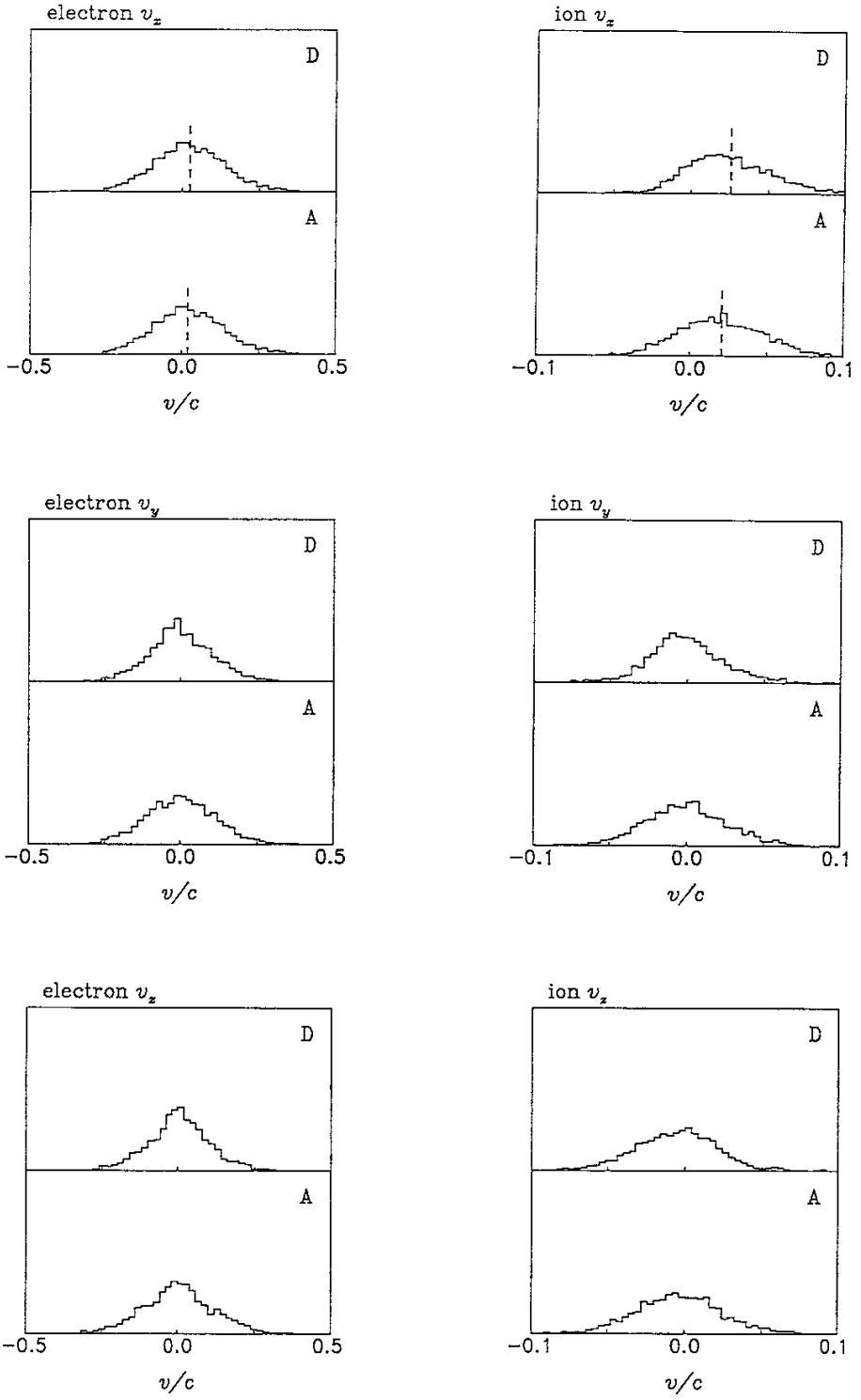
electron v_x
D
A
−0.5
0.0
0.5
v/c
ion v_x
D
A
−0.1
0.0
0.1
v/c
electron v_y
D
A
−0.5
0.0
0.5
v/c
ion v_y
D
A
−0.1
0.0
0.1
v/c
electron v_z
D
A
−0.5
0.0
0.5
v/c
ion v_z
D
A
−0.1
0.0
0.1
v/c

Fig. 10

Recent Issues of NIFS Series

NIFS-47 Yoshi H.Ichikawa, *Solitons and Chaos in Plasma*; Sep. 1990

NIFS-48 T.Seki, R.Kumazawa, Y.Takase, A.Fukuyama, T.Watari, A.Ando, Y.Oka, O.Kaneko, K.Adati, R.Akiyama, R.Ando, T.Aoki, Y.Hamada, S.Hidekuma, S.Hirokura, K.Ida, K.Itoh, S.-I.Itoh, E.Kako, A. Karita, K.Kawahata, T.Kawamoto, Y.Kawasumi, S.Kitagawa, Y.Kitoh, M.Kojima, T.Kuroda, K.Masai, S.Morita, K.Narihara, Y.Ogawa, K.Ohkubo, S.Okajima, T.Ozaki, M.Sakamoto, M.Sasao, K.Sato, K.N.Sato, F.Shinbo, H.Takahashi, S.Tanahashi, Y.Taniguchi, K.Toi and T.Tsuzuki, *Application of Intermediate Frequency Range Fast Wave to JIPP T-IIU Plasma*; Sep.1990

NIFS-49 A.Kageyama, K.Watanabe and T.Sato, *Global Simulation of the Magnetosphere with a Long Tail: The Formation and Ejection of Plasmoids*; Sep.1990

NIFS-50 S.Koide, *3-Dimensional Simulation of Dynamo Effect of Reversed Field Pinch*; Sep. 1990

NIFS-51 O.Motojima, K. Akaishi, M.Asao, K.Fujii, J.Fujita, T.Hino, Y.Hamada, H.Kaneko, S.Kitagawa, Y.Kubota, T.Kuroda, T.Mito, S.Morimoto, N.Noda, Y.Ogawa, I.Ohtake, N.Ohyabu, A.Sagara, T. Satow, K.Takahata, M.Takeo, S.Tanahashi, T.Tsuzuki, S.Yamada, J.Yamamoto, K.Yamazaki, N.Yanagi, H.Yonezu, M.Fujiwara, A.Iiyoshi and LHD Design Group, *Engineering Design Study of Superconducting Large Helical Device*; Sep. 1990

NIFS-52 T.Sato, R.Horiuchi, K. Watanabe, T. Hayashi and K.Kusano, *Self-Organizing Magnetohydrodynamic Plasma*; Sep. 1990

NIFS-53 M.Okamoto and N.Nakajima, *Bootstrap Currents in Stellarators and Tokamaks*; Sep. 1990

NIFS-54 K.Itoh and S.-I.Itoh, *Peaked-Density Profile Mode and Improved Confinement in Helical Systems*; Oct. 1990

NIFS-55 Y.Ueda, T.Enomoto and H.B.Stewart, *Chaotic Transients and Fractal Structures Governing Coupled Swing Dynamics*; Oct. 1990

NIFS-56 H.B.Stewart and Y.Ueda, *Catastrophes with Indeterminate Outcome*; Oct. 1990

NIFS-57 S.-I.Itoh, H.Maeda and Y.Miura, *Improved Modes and the Evaluation of Confinement Improvement*; Oct. 1990

NIFS-58 H.Maeda and S.-I.Itoh, *The Significance of Medium- or Small-size Devices in Fusion Research*; Oct. 1990

NIFS-59 A.Fukuyama, S.-I.Itoh, K.Itoh, K.Hamamatsu, V.S.Chan, S.C.Chiu, R.L.Miller and T.Ohkawa, *Nonresonant Current Drive by RF Helicity Injection*; Oct. 1990

NIFS-60 K.Ida, H.Yamada, H.Iguchi, S.Hidekuma, H.Sanuki, K.Yamazaki and CHS Group, *Electric Field Profile of CHS Heliotron/Torsatron Plasma with Tangential Neutral Beam Injection*; Oct. 1990

NIFS-61 T.Yabe and H.Hoshino, *Two- and Three-Dimensional Behavior of Rayleigh-Taylor and Kelvin-Helmholz Instabilities*; Oct. 1990

NIFS-62 H.B. Stewart, *Application of Fixed Point Theory to Chaotic Attractors of Forced Oscillators;* Nov. 1990

NIFS-63 K.Konn., M.Mituhashi, Yoshi H.Ichikawa,*Soliton on Thin Vortex Filament;* Dec. 1990

NIFS-64 K.Itoh, S.-I.Itoh and A.Fukuyama,*Impact of Improved Confinement on Fusion Research;* Dec. 1990

NIFS -65 A.Fukuyama, S.-I.Itoh and K. Itoh,*A Consistency Analysis on the Tokamak Reactor Plasmas;* Dec. 1990

NIFS-66 K.Itoh, H. Sanuki, S.-I. Itoh and K. Tani,*Effect of Radial Electric Field on α-Particle Loss in Tokamaks;* Dec. 1990

NIFS-67 K.Sato,and F.Miyawaki,*Effects of a Nonuniform Open Magnetic Field on the Plasma Presheath*; Jan.1991

NIFS-68 K.Itoh and S.-I.Itoh,*On Relation between Local Transport Coefficient and Global Confinement Scaling Law;* Jan. 1991

NIFS-69 T.Kato, K.Masai, T.Fujimoto,F.Koike, E.Källne, E.S.Marmar and J.E.Rice,*He-like Spectra Through Charge Exchange Processes in Tokamak Plasmas;* Jan.1991

NIFS-70 K. Ida, H. Yamada, H. Iguchi, K. Itoh and CHS Group, *Observation of Parallel Viscosity in the CHS Heliotron/Torsatron* ; Jan.1991

NIFS-71 H. Kaneko, *Spectral Analysis of the Heliotron Field with the Toroidal Harmonic Function in a Study of the Structure of Built-in Divertor* ; Jan. 1991

NIFS-72 S. -I. Itoh, H. Sanuki and K. Itoh, *Effect of Electric Field Inhomogeneities on Drift Wave Instabilities and Anomalous Transport* ; Jan. 1991

NIFS-73 Y.Nomura, Yoshi.H.Ichikawa and W.Horton, *Stabilities of Regular Motion in the Relativistic Standard Map*; Feb. 1991

NIFS-74 T.Yamagishi, *Electrostatic Drift Mode in Toroidal Plasma with Minority Energetic Particles,* Feb. 1991

NIFS-75 T.Yamagishi, *Effect of Energetic Particle Distribution on Bounce Resonance Excitation of the Ideal Ballooning Mode,* Feb. 1991

NIFS-76 T.Hayashi, A.Tadei, N.Ohyabu and T.Sato, *Suppression of Magnetic Surface Breading by Simple Extra Coils in Finite Beta Equilibrium of Helical System;* Feb. 1991

NIFS-77 N. Ohyabu, *High Temperature Divertor Plasma Operation*; Feb. 1991

NIFS-78 K.Kusano, T. Tamano and T. Sato, *Simulation Study of Toroidal Phase-Locking Mechanism in Reversed-Field Pinch Plasma*; Feb. 1991

NIFS-79 K. Nagasaki, K. Itoh and S. -I. Itoh, *Model of Divertor Biasing and Control of Scrape-off Layer and Divertor Plasmas*; Feb. 1991

NIFS-80 K. Nagasaki and K. Itoh, *Decay Process of a Magnetic Island by Forced Reconnection*; Mar. 1991

NIFS-81 K. Takahata, N. Yanagi, T. Mito, J. Yamamoto, O.Motojima and LHDDesign Group, K. Nakamoto, S. Mizukami, K. Kitamura, Y. Wachi, H. Shinohara, K. Yamamoto, M. Shibui, T. Uchida and K. Nakayama, *Design and Fabrication of Forced-Flow Coils as R&D Program for Large Helical Device*; Mar. 1991

NIFS-82 T. Aoki and T. Yabe, *Multi-dimensional Cubic Interpolation for ICF Hydrodynamics Simulation*; Apr. 1991

NIFS-83 K. Ida, S.-I. Itoh, K. Itoh, S. Hidekuma, Y. Miura, H. Kawashima, M. Mori, T. Matsuda, N. Suzuki, H. Tamai, T.Yamauchi and JFT-2M Group, *Density Peaking in the JFT-2M Tokamak Plasma with Counter Neutral Beam Injection* ; May 1991

NIFS-84 A. Iiyoshi, *Development of the Stellarator/Heliotron Research*; May 1991

NIFS-85 Y. Okabe, M. Sasao, H. Yamaoka, M. Wada and J. Fujita, *Dependence of Au^- Production upon the Target Work Function in a Plasma-Sputter-Type Negative Ion Source;* May 1991

NIFS-86 N. Nakajima and M. Okamoto, *Geometrical Effects of the Magnetic Field on the Neoclassical Flow, Current and Rotation in General Toroidal Systems*; May 1991

NIFS-87 S. -I. Itoh, K. Itoh, A. Fukuyama, Y. Miura and JFT-2M Group, *ELMy-H mode as Limit Cycle and Chaotic Oscillations in Tokamak Plasmas;* May 1991

NIFS-88 N.Matsunami and K.Kitoh, *High Resolution Spectroscopy of H^+ Energy Loss in Thin Carbon Film;* May 1991

NIFS-89 H. Sugama, N. Nakajima and M.Wakatani, *Nonlinear Behavior of Multiple-Helicity Resistive Interchange Modes near Marginally Stable States;* May 1991

NIFS-90 H. Hojo and T.Hatori, *Radial Transport Induced by Rotating RF Fields and Breakdown of Intrinsic Ambipolarity in a Magnetic Mirror*; May 1991

NIFS-91 M. Tanaka, S. Murakami, H. Takamaru and T.Sato, *Macroscale Implicit, Electromagnetic Particle Simulation of Inhomogeneous and Magnetized Plasmas in Multi-Dimensions;* May 1991

NIFS-92 S. - I. Itoh, *H-mode Physics, -Experimental Observations and Model Theories-, Lecture Notes, Spring College on Plasma Physics, May 27 - June 21 1991 at International Centre for Theoretical Physics (IAEA UNESCO) Trieste, Italy ;* Jun. 1991

NIFS-93 Y. Miura, K. Itoh, S. - I. Itoh, T. Takizuka, H. Tamai, T. Matsuda, N. Suzuki, M. Mori, H. Maeda and O. Kardaun, *Geometric Dependence of the Scaling Law on the Energy Confinement Time in H-mode Discharges;* Jun. 1991

NIFS-94 H. Sanuki, K. Itoh, K. Ida and S. - I. Itoh, *On Radial Electric Field Structure in CHS Torsatron / Heliotron;* Jun. 1991

NIFS-95 K. Itoh, H. Sanuki and S. - I. Itoh, *Influence of Fast Ion Loss on Radial Electric Field in Wendelstein VII-A Stellarator;* Jun. 1991

NIFS-96 S. - I. Itoh, K. Itoh, A. Fukuyama, *ELMy-H mode as Limit Cycle and Chaotic Oscillations in Tokamak Plasmas;* Jun. 1991

NIFS-97 K. Itoh, S. - I. Itoh, H. Sanuki, A. Fukuyama, *An H-mode-Like Bifurcation in Core Plasma of Stellarators;* Jun. 1991

NIFS-98 H. Hojo, T. Watanabe, M. Inutake, M. Ichimura and S. Miyoshi, *Axial Pressure Profile Effects on Flute Interchange Stability in the Tandem Mirror GAMMA 10;* Jun. 1991

NIFS-99 A. Usadi, A. Kageyama, K. Watanabe and T. Sato, *A Global Simulation of the Magnetosphere with a Long Tail : Southward and Northward IMF;* Jun. 1991

NIFS-100 H. Hojo, T. Ogawa and M. Kono, *Fluid Description of Ponderomotive Force Compatible with the Kinetic One in a Warm Plasma* ; July 1991

NIFS-101 H. Momota, A. Ishida, Y. Kohzaki, G. H. Miley, S. Ohi, M. Ohnishi K. Yoshikawa, K. Sato, L. C. Steinhauer, Y. Tomita and M. Tuszewski *Conceptual Design of D-^{3}He FRC Reactor "ARTEMIS"* ; July 1991

NIFS-102 N. Nakajima and M. Okamoto, *Rotations of Bulk Ions and Impurities in Non-Axisymmetric Toroidal Systems* ; July 1991

NIFS-103 A. J. Lichtenberg, K. Itoh, S. - I. Itoh and A. Fukuyama, *The Role of Stochasticity in Sawtooth Oscillation* ; Aug. 1991

NIFS-104 K. Yamazaki and T. Amano, *Plasma Transport Simulation Modeling for Helical Confinement Systems;* Aug. 1991

NIFS-105 T. Sato, T. Hayashi, K. Watanabe, R. Horiuchi, M. Tanaka, N. Sawairi and K. Kusano, *Role of Compressibility on Driven Magnetic Reconnection ;* Aug. 1991

NIFS-106 Qian Wen - Jia, Duan Yun - Bo, Wang Rong - Long and H. Narumi, *Electron Impact Excitation of Positive Ions - Partial Wave Approach in Coulomb - Eikonal Approximation* ; Sep. 1991